Weierstraß-Institut
für Angewandte Analysis und Stochastik

Leibniz-Institut im Forschungsverbund Berlin e. V.

Preprint ISSN 2198-5855

On forward and inverse uncertainty quantification for a model for a magneto mechanical device involving a hysteresis operator

Carmine Stefano Clemente[1], Daniele Davino[1], Olaf Klein[2], Ciro Visone[3]

submitted: April 18, 2023

[1] Università degli Studi del Sannio
P.zza Roma, 21
82100 Benevento
Italy
E-Mail: carmine.clemente@unisannio.it
davino@unisannio.it

[2] Weierstrass Institute
Mohrenstr. 39
10117 Berlin
Germany
E-Mail: olaf.klein@wias-berlin.de

[3] Università di Napoli Federico II
Via Claudio, 21
80125 Napoli
Italy
E-Mail: ciro.visone2@unina.it

No. 3009
Berlin 2023

2020 *Mathematics Subject Classification.* 47J40, 60H30.

Key words and phrases. Hysteresis, uncertainty quantification (UQ), magnetostrictive material, Bayesian inverse problems (BIP).

The third author would like to thank Prof. Claudia Schillings, Freie Universität Berlin, Germany, Prof. Tim Sullivan, University of Warwick, Coventry, United Kingdom, and Dr. Paul-Remo Wagner, ETH Zurich, Switzerland for fruitful discussions.

Edited by
Weierstraß-Institut für Angewandte Analysis und Stochastik (WIAS)
Leibniz-Institut im Forschungsverbund Berlin e. V.
Mohrenstraße 39
10117 Berlin
Germany

Fax: +49 30 20372-303
E-Mail: preprint@wias-berlin.de
World Wide Web: http://www.wias-berlin.de/

On forward and inverse uncertainty quantification for a model for a magneto mechanical device involving a hysteresis operator

Carmine Stefano Clemente, Daniele Davino, Olaf Klein, Ciro Visone

Abstract

Modeling real world objects and processes one may has to deal with hysteresis effects but also with uncertainties. Following D. Davino, P. Krejčí, and C. Visone: Fully coupled modeling of magneto-mechanical hysteresis through 'thermodynamic' compatibility. *Smart Mater. Struct.*, 22(9), (2013) 0950099, a model for a magnetostrictive material involving a generalized Prandtl-Ishlinskiĭ-operator is considered here.

Using results of measurements, some parameters in the model are determined and inverse Uncertainty Quantification (UQ) is used to determine random densities to describe the remaining parameters and their uncertainties. Afterwards, the results are used do perform forward UQ and to compare the results with measured data. This extends some of the results from O. Klein, D. Davino, and C. Visone. On forward and inverse uncertainty quantification for models involving hysteresis operators. *Math. Model. Nat. Phenom.* 15 (2020) 53.

1 Uncertainty quantification and hysteresis: motivation and topics

1.1 Uncertainties in models with hysteresis operators

Considering magnetization, piezo-electric effects, elasto-plastic behavior, or magnetostrictive materials, one has to take into account hysteresis effects. Many models involve therefore *hysteresis operators* and are also subject to *uncertainties*:

- Parameters in the models are identified using results from *measurements*. Hence, they can be influenced by *measurement errors*.
- Parameters being identified for some *sample specimens* are also used for other specimens.
- Material/device may change after performing the measurements, for example, due to temperature changes or aging.
- Moreover, if one is performing several measurements, there can be conditions not considered in the model that change between the measurements, creating quite different measurement results that corresponds to different parameter values in the used model.

The parameters in the hysteresis operators used to model hysteresis effects are therefore also subject to uncertainties. In the following, methods of *Uncertainty Quantification (UQ)*, will be applied to describe/determine the uncertainties and to investigate their influence.

DOI 10.20347/WIAS.PREPRINT.3009 Berlin 2023

1.2 Uncertainty quantification

Following e.g. [17, 18], we consider as *Uncertainty Quantification (UQ)*: Use of probability theory to deal with uncertainties, i.e. parameters with uncertain values are represented by random variables modeling the information/assumptions/beliefs on the values and the uncertainties of the parameter values. In the current paper, the following aspects of UQ will be discussed:

Forward UQ Starting from representations of the uncertain parameter values by random variables, one considers the model output as random variable and computes properties like expected value, variation, probabilities for outputs entering some interval, credible intervals, and other *Quantities of Interest (QoI)*.

Inverse UQ Using data and measurements to determine values and the uncertainty of the parameters, i.e. to determine a random variable taking into account the information provided by the data and the measurements, and use the random variable to represent the parameters afterwards.

Other subjects of/related to UQ, like *sensitivity analysis*, where one is investigating which input parameters have the largest effect (in terms of uncertainty) on the output quantity, will not be discussed here.

1.3 UQ for a model for magneto-mechanical components — Topic of this paper

A model with a hysteresis operator is used to describe a magnetostrictive actuator. Using measurements for this actuator, parameters in the hysteresis operator and their uncertainty are identified by inverse UQ. Afterwards, forward UQ is performed.

This work extends results from Section 5 in [7].

2 Hysteresis operators

2.1 Hysteresis operators - general definition

In this section, we assume that some $T > 0$ is given.

Following [2, 10, 19], we define:

Definition 2.1. Let non-empty sets X, Y be given. Let $\mathcal{H} : D(\mathcal{H}) \to \mathrm{Map}([0,T], Y)$ with $\emptyset \neq D(\mathcal{H}) \subseteq \mathrm{Map}([0,T], X)$ be given.

a) $\mathcal{H}$ is a *hysteresis operator* $:\Longleftrightarrow \mathcal{H}$ is rate-independent and causal.

b) $\mathcal{H}$ is *rate-independent* $:\Longleftrightarrow \forall\, v \in D(\mathcal{H}), \forall\, \alpha : [0,T] \to [0,T]$ being continuous and increasing (not necessary strictly increasing), with $\alpha(0) = 0$, $\alpha(T) = T$, and $v \circ \alpha \in D(\mathcal{H})$ it holds: $\mathcal{H}[v \circ \alpha] = \mathcal{H}[v] \circ \alpha$.

c) $\mathcal{H}$ is *causal* $:\Longleftrightarrow \forall\, v_1, v_2 \in D(\mathcal{H}), \forall\, t \in [0,T]$: If $v_1(\tau) = v_2(\tau) \quad \forall\, \tau \in [0,t]$ then $\mathcal{H}[v_1](t) = \mathcal{H}[v_2](t)$.

2.2 The play-operator – definition and properties

Definition 2.2. Considering some *yield limit* $r \geq 0$ and some *initial state* z, the *play-operator* $\mathcal{P}_r[z,\cdot]$ maps $u \in C([0,T];\mathbb{R})$ being piecewise monotone to $\mathcal{P}_r[z,u] \in C([0,T];\mathbb{R})$ which is also piecewise monotone and it holds (see e.g. [2, 9, 10, 19])

$$\mathcal{P}_r[z,u](0) = \max\left(u(0)-r, \min\left(u(0)+r, z\right)\right), \tag{2.1}$$

$$\mathcal{P}_r[z,u](t) = \begin{cases} \max\left(\mathcal{P}_r[z,u](t_*), u(t)-r\right), & \text{if } u \text{ is increasing on } [t_0,t], \\ \min\left(\mathcal{P}_r[z,u](t_*), u(t)+r\right), & \text{if } u \text{ is decreasing on } [t_*,t], \end{cases} \tag{2.2}$$

for all $t_*, t \in [0,T]$ with $t_* < t$ such that u **is monotone on** $[t_*,t]$**.**

As an example, we consider the evolution of $\mathcal{P}_2[0,u]$ for some input function u combined with plots for $u+2$ and $u-2$ as shown in Fig. 1. Moreover, the corresponding input-output diagram, showing the evolution of $(u, \mathcal{P}_2[0,u])$, is presented in Fig. 2.

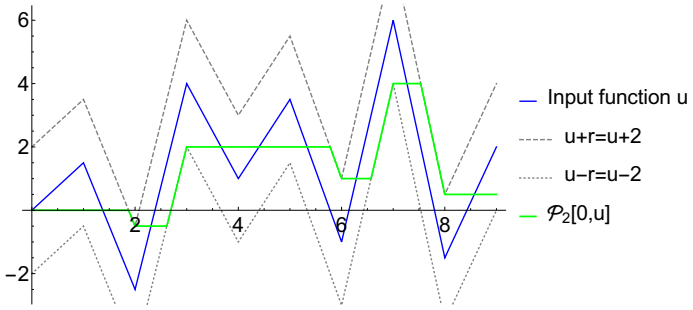

Figure 1: Evolution of the input $u(t)$, of $u(t)-2$, of $u(t)+2$ and of the output of the play-operator $\mathcal{P}_2[0,u](t)$.

Remark 2.3. Using e.g. [2, 9, 10, 19], one can show:

a) It holds for all $r \geq 0$ and all $z \in \mathbb{R}$: the play-operator defined above can be continuously extended to the well known and well defined *play-operator* $\mathcal{P}_r[z,\cdot]$ from $\mathrm{C}([0,T];\mathbb{R})$ to $\mathrm{C}([0,T];\mathbb{R})$, being also a hysteresis operator.

b) Let $\lambda_0 : [0,\infty) \to \mathbb{R}$ being Lipschitz-continuous with Lipschitz constant 1 be given such that there exists some $R > 0$ with $\lambda_0(r) = 0$ for all $r \geq R$. Then it hold for all $u \in \mathrm{C}([0,T];\mathbb{R})$ and all $t \in [0,T]$: the mapping $\mathcal{P}.[\lambda_0(\cdot),u](t) : [0,\infty) \to \mathbb{R}$ defined by $[0,\infty) \ni r \mapsto \mathcal{P}_r[\lambda_0(r),u](t)$ is continuous and there is some $R_{u,t} > 0$ such that $\mathcal{P}_r[\lambda_0(r),u](t) = 0$ for all $r > R_{u,t}$.

2.3 Prandtl-Ishlinskiĭ-operator

Following [2, 9, 10, 19], we define:

Definition 2.4. Let $\zeta \in L^1_{loc}([0,\infty))$ be given.

a) Let $\lambda_0 : [0,\infty) \to \mathbb{R}$ being Lipschitz-continuous with Lipschitz constant 1 be given such that there exists some $R > 0$ with $\lambda_0(r) = 0$ for all $r \geq R$. Let $\mathcal{PI}_\zeta[\lambda_0,\cdot] : C([0,T];\mathbb{R}) \to C([0,T];\mathbb{R})$

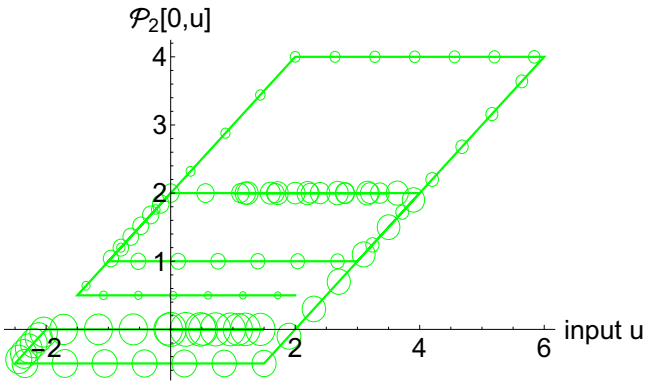

Figure 2: Input-output-diagram, derived using the data leading to Fig. 1. Therein, the evolution of $(u(t), \mathcal{P}_2[0,u](t))$ is shown.

be the *Prandtl-Ishlinskiĭ-operator for the weight function* ζ *and the initial state function* λ_0 defined by mapping $u \in C([0,T];\mathbb{R})$ to the function $\mathcal{PI}_\zeta[\lambda_0, u] \in C([0,T];\mathbb{R})$ with

$$\mathcal{PI}_\zeta[\lambda_0, u](t) = \int_0^\infty \zeta(r)\mathcal{P}_r[\lambda_0(r), u](t)\,\mathrm{d}r\,, \quad \forall\, t \in [0,T]. \tag{2.3}$$

b) The *Prandtl-Ishlinskiĭ-operator* $\mathcal{PI}_\zeta[0,\cdot]$ *for the weight function* ζ *and the trivial initial state* is defined as the operator in a) with $\lambda_0 \equiv 0$ on $[0,\infty)$.

c) The *Prandtl-Ishlinskiĭ-operator* $\mathcal{PI}_\zeta[\cdot,\cdot]$ *for the weight function* ζ maps (λ_0, u) with λ_0 as in a) and $u \in C([0,T];\mathbb{R})$ to $\mathcal{PI}_\zeta[\lambda_0, u]$ as in a).

d) The *initial loading curve* $\Psi_{\mathcal{PI},\zeta}(s)$ *for the Prandtl-Ishlinskiĭ-operator* $\mathcal{PI}_\zeta[\cdot,\cdot]$ is defined by requesting that for all $\beta \in \mathbb{R}$:

$$\Psi_{\mathcal{PI},\zeta}(\beta) := \mathcal{PI}_\zeta[0, u_\beta](T) \quad \text{with} \quad u_\beta \in C([0,T];\mathbb{R}) \quad \text{defined by } u_\beta(t) = \beta/T, \quad \forall\, t \in [0,T]. \tag{2.4}$$

Remark 2.5. Let $\zeta \in L^1_{loc}([0,\infty))$ be given. For the initial loading curve $\Psi_{\mathcal{PI},\zeta}$ for the Prandtl-Ishlinskiĭ-operator $\mathcal{PI}_\zeta[\cdot,\cdot]$ it holds for all $s \in \mathbb{R}$ that

$$\Psi_{\mathcal{PI},\zeta}(s) = \begin{cases} \int_0^s \zeta(r)(s-r)\,\mathrm{d}r\,, & \text{if } s > 0, \\ 0, & \text{if } s = 0, \\ \int_0^{-s} \zeta(r)(s+r)\,\mathrm{d}r\,, & \text{if } s < 0, \end{cases} \qquad = -\Psi_{\mathcal{PI},\zeta}(-s). \tag{2.5}$$

2.4 Identification of initial loading curve from measurements

Remark 2.6. Using [11, 14, 4], one can show:

For $u \in C([0,T];\mathbb{R})$ and $0 \le t_a < t_b < t_c \le T$ with u being monotone on $[t_a, t_b]$ and on $[t_b, t_c]$ and $u(t_a) = u(t_c)$ it holds that

$$\forall\, t \in [t_b, t_c]: \quad \Psi_{\mathcal{PI},\zeta}\left(\frac{u(t) - u(t_b)}{2}\right) = \frac{1}{2}\left(\mathcal{PI}_\zeta[\lambda_0, u](t) - \mathcal{PI}_\zeta[\lambda_0, u](t_b)\right). \tag{2.6}$$

Remark 2.7. If one is considering some process mapping time-dependent input functions to some measurable time-dependent output quantity Q, then one may like to model this by applying a Prandtl-Ishlinskiĭ-operator. To identify a corresponding weight function, one can use a function u with a cycle as in Remark 2.6 as an input to this process and determine given/measured values for u and Q at times $s_0 < s_1 < \cdots < s_K$ with $t_b = s_0$ and $s_K = t_c$. Hence, one gets $0 = v_0 < v_1 < \cdots < v_K$ and $\psi_0, \psi_1, \ldots, \psi_K \in \mathbb{R}$ defined by

$$v_i := \left| \frac{u(s_i) - u(s_0)}{2} \right|, \qquad \psi_i := \frac{1}{2} \begin{cases} Q(s_i) - Q(s_0), & \text{if} \quad u(s_K) \geq u(s_0), \\ Q(s_0) - Q(s_i), & \text{if} \quad u(s_K) \leq u(s_0). \end{cases} \tag{2.7}$$

By recalling (2.6), we see that one is looking for some weight function ζ with

$$\Psi_{\mathcal{PI},\zeta}(v_i) \approx \psi_i, \quad \forall\, i \in \{0, \ldots, K\}. \tag{2.8}$$

Since the definition yields that $v_0 = 0$ and $\psi_0 = 0$, we deduce from (2.5) that the equation in (2.8) is satisfied for $k = 0$ for all admissible weight functions ζ, such that for determining ζ one can ignore $k = 0$ in (2.8) .

Remark 2.8. Starting from data as in Remark 2.7 one can derive an approximation for an initial loading curve on $[0, v_K]$ by considering a function Ψ that is linear on $[v_0, v_1]$, $[v_1, v_2], \ldots,$ $[v_{K-1}, v_K]$ and satisfies $\Psi(v_k) = \psi_k$ for all $k \in \{0, \ldots, K\}$.

Remark 2.9. The considerations in Remark 2.7 can be extended to the following situation: one is considering a function $u \in C([0,T]; \mathbb{R})$ and $t_b, t_c \in [0,T]$ with $t_b < t_c$ such that u is monotone on $[t_b, t_c]$ and one is able to show somehow that the equation in (2.6) is at least approximately valid for all $t \in [t_b, t_c]$.

3 Uncertainties in a model for magneto-mechanical components

3.1 General considerations

In [3, Sec. 5], a model for magneto-mechanical devices has been derived. Therein, a *generalized Prandtl-Ishlinskiĭ-operator*, see also [8, 20],

$$\mathcal{G}_{c_1,c_2,c_3}[\lambda_0, H](t) := \mathcal{PI}_{\zeta_{c_1,c_2}}[\lambda_0, \tanh(c_3 H)](t) \tag{3.1}$$

with $\zeta_{c_1,c_2}(r) := c_1 \mathrm{e}^{-r/c_2}$ for all $r \geq 0$, $c_1, c_2, c_3 > 0$ and $\lambda_0 : [0, \infty] \to \mathbb{R}$ satisfying the conditions discussed above is considered. In [3], it is shown that this operator provides an approximation for the *magnetization* of Galfenol for an applied magnetic field H; with c_3 depending on the applied stress.

In the following, we will assume that the applied magnetic field H is proportional to the applied current I such that we can consider $\mathcal{G}_{c_1,c_2,c_3}[\lambda_0, I]$ (with an appropriate updated value for c_3) instead of $\mathcal{G}_{c_1,c_2,c_3}[\lambda_0, H]$.

The initial loading curve $\Psi_{\mathcal{PI},\zeta_{c_1,c_2}}$ for $\mathcal{PI}_{\zeta_{c_1,c_2}}$ satisfies

$$\Psi_{c_1,c_2}(s) := \Psi_{\mathcal{PI},\zeta_{c_1,c_2}}(s) = s c_1 c_2 + c_1 c_2^2 \left(\mathrm{e}^{-\frac{s}{c_2}} - 1 \right), \quad \forall s \geq 0. \tag{3.2}$$

In [1], a magnetostrictive Terfenol-actuator is investigated and the hysteresis between the current generating the magnetic field and the resulting displacement is considered. In this paper, data creating a *First-Order-Reversal-Curves (FORC)*–diagram quite similar to the one in Fig. 3 were used to determine the parameter field/values in a Preisach-operator and a generalized Prandtl-Ishlinskiĭ-operator.

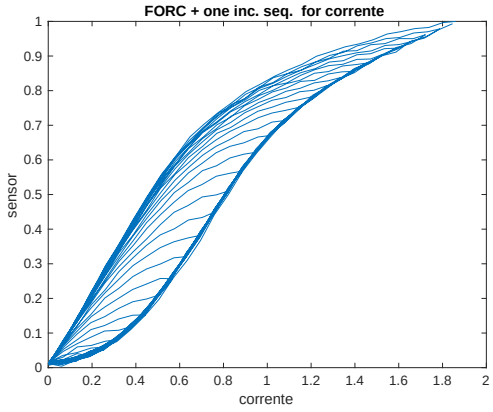

Figure 3: A FORC-diagram for a magnetostrictive Terfenol-actuator similar to the one considered in [1], and one additional curve derived for increasing current.

3.2 Considerations and results in [7, Sec. 5]

The data used to prepare the FORC-diagram in Fig. 3 and one additional data set with increasing current measured directly afterward are shown in Fig. 4. In [7, Sec. 5], these data have been used to identify parameter values $c_1, c_2, c_3 > 0$ such that the generalized Prandtl-Ishlinskiĭ-operator $\mathcal{G}_{c_1,c_2,c_3}[\lambda_0, I](t)$ creates approximations for these data. The resulting value for $c_3 = c_{\tanh} = 0.682138$ will be used in the following. Moreover, the uncertainties for c_1 and c_2 were also investigated.

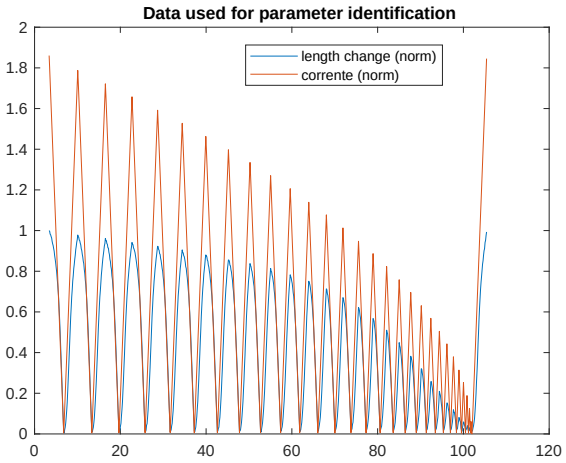

Figure 4: Measured data used to generate the FORC-diagram in Fig. 3, and one additional data set with increasing current (corrente) measured directly afterward.

In the following, we will denote the times of local extrema for the current I by $t_0, t_1, \ldots, t_{58}$ and L will be the relative length change determined from measurements of a corresponding sensor. Thanks to the measurements, we have values for I and L at times $s_{0,j}, s_{1,j}, \ldots s_{K_j^*,j} \in [t_{j-1}, t_j]$ with $t_{j-1} =$

$s_{0,j} < s_{1,j} < \cdots < s_{K_j^*,j} = t_j$ for all $j \in \{1, \dots, 58\}$ and

$$K_1^* = 29, \quad K_2^* = K_3^* = 28,\ K_4^* = K_5^* = 27,\ \dots, K_{54}^* = K_{55}^* = 2, \quad K_{56} = 1,\ K_{57} = 2, K_{58} = 29. \tag{3.3}$$

In the following, we will use results from a reformulation of Section 2 by replacing therein every "$[0,T]$" with "$[t_0, t_{58}]$", "$\alpha(0) = 0$" and "$\alpha(T) = T$" in Definition 2.1.b) with "$\alpha(t_0) = t_0$" and "$\alpha(t_{58}) = t_{58}$", respectively, "$[0,t]$" in Definition 2.1.c) with "$[t_0, t]$", "0" in (2.1) with "t_0", and "$0 \le t_a < t_b < t_c \le T$" in Remark 2.6 with "$t_0 \le t_a < t_b < t_c \le t_{58}$".

Considering any $j \in \{2, \dots, 57\}$ and investigating the evolution of $u := \tanh(c_3 I)$ on $[t_{j-2}, t_{j-1}]$ and on $[t_{j-1]}, t_j]$, we see that one is dealing with the situation discussed in Remark 2.6 with $t_{j-2} =: t_a$, $t_{j-1} =: t_b$ and $t_j =: t_c$.

For any $i \in \{1, \dots, 28\}$, we see that u is increasing on $[t_{2i-1}, t_{2i}] = [s_{0,2i}, s_{K_i,2i}]$ with $K_i := K_{2i}^*$. Hence, by following Remark 2.7, we can compute $v_{0,i}, \dots, v_{K_i,i}$ and $\psi_{0,i}, \dots, \psi_{K_i,i}$ defined by

$$v_{k,i} := \frac{1}{2} \left| \tanh\left(c_3 I(s_{k,2i})\right) - \tanh\left(c_3 I(s_{1,2i})\right) \right| = \frac{1}{2} \left(\tanh\left(c_3 I(s_{k,2i})\right) - \tanh\left(c_3 I(s_{1,2i})\right) \right), \tag{3.4a}$$

$$\psi_{k,i} := \frac{1}{2} \left(L\left(s_{k,2i}\right) - L\left(s_{1,2i}\right) \right), \tag{3.4b}$$

for $k = 0, \dots, K_i$. Now, in view of (2.6) and (2.8), one would like to find some density ζ_i for the Prandtl-Ishlinskiĭ-operator such that $\Psi_{\mathcal{PI},\zeta_i}\left(v_{k,i}\right) \approx \psi_{k,i}$ for all $k \in \{0, \dots, K_i\}$.

Moreover, one can either combine the return point memory property of the Prandtl-Ishlinskiĭ operator with its continuity or investigate the graphs $[0,\infty) \ni r \mapsto \mathcal{P}_r[\lambda_0(r), u](t)$ and compute the resulting integrals to show for $t_b := t_{57}$ and $t_c := t_{58}$ that one is in a situation as in Remark 2.9. Hence, we can derive the equation above also for $i = 29$.

For any $i \in \{31, \dots, 58\}$, we see that u is decreasing on $[t_{2(i-30)}, t_{2(i-30)+1}] = [s_{0,2(i-30)+1}, s_{K_i,2(i-30)+1}]$ with $K_i := K_{2(i-30)+1}^*$ and that we are in the situation discussed in Remark 2.6. Hence, by following this remark, we can compute $v_{0,i}, \dots, v_{K_i,i}$ and $\psi_{0,i}, \dots, \psi_{K_i,i}$ by

$$\begin{aligned} v_{k,i} &:= \frac{1}{2} \left| \tanh\left(c_3 I(s_{k,2(i-30)+1})\right) - \tanh\left(c_3 I(s_{0,2(i-30)+1})\right) \right| \\ &= \frac{1}{2} \left(\tanh\left(c_3 I(s_{0,2(i-30)+1})\right) - \tanh\left(c_3 I(s_{k,2(i-30)+1})\right) \right), \end{aligned} \tag{3.5a}$$

$$\psi_{k,i} := \frac{1}{2} \left(L\left(s_{0,2(i-30)+1}\right) - L\left(s_{k,2(i-30)+1}\right) \right), \tag{3.5b}$$

for $k = 0, \dots, K_i$. Now, again in view of (2.6) and (2.8), one would like to find some density ζ_i for the Prandtl-Ishlinskiĭ-operator such that $\Psi_{\mathcal{PI},\zeta_i}\left(v_{k,i}\right) \approx \psi_{k,i}$ for all $k \in \{0, \dots, K_i\}$.

Moreover, since the experiment is supposed to generate measurements allowing to generate a FORC-diagram, we can assume that the preparation phase of the measurement has been done in such a way that (2.6) is valid with $t_b := t_0 = t_{2(30-30)}$ and $t_c := t_1 = t_{2(30-30)+1}$, such that we can also perform the above considerations for $i = 30$.

Combining the above considerations, it holds for any $j \in \{1, \dots, 58\}$ that we have determined K_j, $v_{0,j}, \dots, v_{K_j,j}$ and $\psi_{0,j}, \dots, \psi_{K_j,j}$ such that one would like to find some density ζ_j for the Prandtl-Ishlinskiĭ-operator satisfying

$$\Psi_{\mathcal{PI},\zeta_j}\left(v_{k,j}\right) \approx \psi_{k,j}, \qquad \forall\, k \in \{0, \dots, K_j\}. \tag{3.6}$$

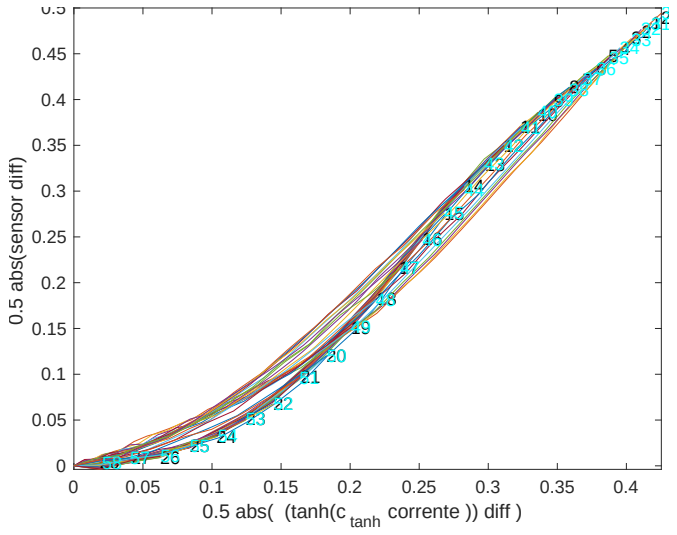

Figure 5: For every $i \in \{1, 2, \ldots, 58\}$ the approximation of an initial loading curve generated from the points $(v_{0,i}, \psi_{0,i}), (v_{1,i}, \psi_{1,i}), \ldots, (v_{K_i,i}, \psi_{K_i,i})$ following Remark 2.8 is shown.

Following Remark 2.8, we can also derive an approximation for an initial loading curve from this data set. In Figure 5, these approximations are shown.

As pointed out before (2.8), for determining ζ_j we can ignore $k = 0$ in the above equation. If one is only interested in dealing with densities as in Section 3.1, one has $\zeta_j = \zeta_{c_{1,j},c_{2,j}}$ with appropriate values $c_{1,j}, c_{2,j} \in (0, \infty)$ such that it holds, thanks to (3.2),

$$\Psi_{c_{1,j},c_{2,j}}(v_{k,j}) \approx \psi_{k,j}, \qquad \forall\, k \in \{1, \ldots, K_j\}. \tag{3.7}$$

Remark 3.1. In [7, Sec. 5] appropriate pairs $(c_{1,KDV,1}, c_{2,KDV,1}), (c_{1,KDV,2}, c_{2,KDV,2}), \ldots, (c_{1,KDV,58}, c_{2,KDV,58})$ were computed such that (3.7) is satisfied for $c_{1,j} = c_{1,KDV,j}$ and $c_{2,j} = c_{2,KDV,j}$ for all $j \in \{1, \ldots, 58\}$.

Afterwards, a simple inverse UQ calculation was performed: for a subset $((c_{1,KDV,i}, c_{2,KDV,k}))_{i=30}^{55}$ of nice parameter pairs the discrete mean and the standard deviation were calculated. Afterwards, c_1 and c_2 were represented by independent random variables with the corresponding normal distributions truncated to $[0.0000001, \infty]$ and some forward UQ computations were performed.

Performing a further simple inverse UQ by also computing the discrete mean and the discrete standard deviation using all pairs $((c_{1,KDV,i}, c_{2,KDV,k}))_{i=1}^{58}$, it turned out that the discrete mean for c_2 was 4.71742 and the discrete standard deviation for c_2 was 7.94603, such that using a truncated normally distributed distribution does not seem to be an appropriate description for c_2. Moreover, it turned out that the values in $((c_{1,KDV,i}, c_{2,KDV,k}))_{i=1}^{58}$ show a significant correlation and considering their distribution (see [7, Fig 14]), it became obvious that these pairs do not represent samples of two independent truncated normally distributed random variables.

Also, the values in the subset $((c_{1,KDV,i}, c_{2,KDV,k}))_{i=30}^{55}$ of nice parameter pairs show a significant correlation and investigating the distribution of these pairs, see [7, Fig 15], it became obvious that these pairs also do not represent samples of two independent truncated normally distributed random variables.

Because of these observations, it was tried in [7, Sec. 5] to find a random variable on $(0, \infty)^2$ such that the above pairs could be typical samples for this random variable, by applying a formulation of Bayes' Theorem as in [6, Theorem 3.1], see also Sec. 3.4.

3.3 Likelihood and Bayes' Theorem

The following definition of the likelihood (compare, e.g. [17, 16, 6]) is quite often applied in situations with V_q being equal to the value of some model evaluated at q with additional noise that is normally distributed with mean 0.

Definition 3.2. Let $m, n \in \mathbb{N}$ be given. Let $Q \subset \mathbb{R}^m$ be a set of parameter values. Assume that for every $q \in Q$ we have a continuous $\mathbb{R}^n$-valued random variable V_q with probability density $\rho(\cdot; q)$ on $\mathbb{R}^n$.

For all $q \in Q$ and all $v \in \mathbb{R}^n$ it holds that the *likelihood* $L(q|v)$ is defined by

$$L(q|v) := \rho(v; q) = \rho(V_q = v; q). \tag{3.8}$$

The *likelihood function* $L(\cdot|v)$ for v is mapping $q \in Q$ to $L(q|v)$.

This combination of assumptions with be used in the following:

Assumption 3.3. Assume that we are in the situation of Definition 3.2 and that integrals on Q are well defined. Assume that a known probability density π_0 on Q, denoted as *prior density*, is given. Assume that some $v_{obs} \in \bigcup_{q\in Q} V_q$ is given, such that $\int_Q L\left(q'|v_{obs}\right) \pi_0(q') \mathrm{d}\, q' > 0$.

Having a close look at the proof of [6, Theorem 3.1], one realizes that the first equation on page 51 only holds if the prior density is just the density of the to be identified random variable representing the parameters. Adapting now the formulation of *Bayes' Theorem of Inverse Problems* such that the proof is valid, one ends up with the following Theorem allowing to compute the solution of the corresponding *Bayesian inverse problems (BIP)* with (3.9). Similar formulations can also be found, e.g. in [17, Res. 8.1] or [12, Sec. 2.1.2].

Theorem 3.4. *Assume that Assumption 3.3 is satisfied and that a random variable X_0 with values in Q is given such that π_0 is its probability density, that v_{obs} can be considered as a sample of V_{X_0}.and that there exists a joint probability density for X_0 and V_{X_0}.*

A Baysian's belief π_{new} combining the information in X_0 and in the observed datum v_{obs} is the posterior probability density $\pi_{new}\left(\cdot|V_{X_0} = v_{obs}\right)$ of X_0, given the data v_{obs}*, and it holds that*

$$\pi_{new}\left(q|V_{X_0} = v_{obs}\right) = \frac{L\left(q|v_{obs}\right)\pi_0(q)}{\int_Q L\left(q'|v_{obs}\right)\pi_0(q')\mathrm{d}\, q'}, \quad \forall\, q \in X_0. \tag{3.9}$$

In [18, Sec 6.22], the formulation is adjusted to the situation that Q is a subset of a general separable Banach space and V_q is of the form described before Definition 3.2.

As one can see, the derived density does not depend on X_0, such that the following theorem is proved.

Theorem 3.5. *Assume that Assumption 3.3 is satisfied and that a random variable X_0 with values in Q exits such that the assumptions in Theorem 3.4 are satisfied.*

A Baysian's belief combining the information in π_0 and in the observed datum v_{obs} by using Bayes' Theorem of Inverse Problems is the posterior probability density for the prior density π_0, given the data v_{obs} *which is defined as the posterior probability density $\pi_{new}\left(\cdot|V_{X_0} = v_{obs}\right)$ of X_0, given the data v_{obs} as in Theorem 3.4.*

Remark 3.6. Assume that Assumption 3.3 is satisfied and that we try to identity some fixed, true, and unknown value $q_{true} \in Q$. Assume that the informations/beliefs on the value of q_{true} in advance of an observation are summarized by the *prior* probability density π_0 on Q. Assume that v_{obs} is some sample of $V_{q_{true}}$ that has been observed. A Baysian's belief combining the information in π_0 and in the observed datum v_{obs} by using Bayes' Theorem of Inverse Problems as in Theo. 3.5 is the *posterior probability density for the prior density π_0, given the data v_{obs}* which is defined following Theorem 3.5, if it holds that there exists a random variable X_0 with values in Q such that the assumptions in Theorem 3.4 are satisfied. (This implies that we need to request that v_{obs} is also a sample of V_{X_0}.)

Remark 3.7. For the "identification of a true value" formulation of Bayes' Theorem as in Remark 3.6 it holds that by subsequently applying the theorem for different observations, using the last computed posterior density as new prior density, one can show some kind of convergence of the computed densities to the true value with the Bernstein-von Mises Theorem (see, e.g., [18, Theorm 6.17]).

Hence, this yields that in most situations the posterior density computed by Bayes' Theorem provides a better approximation to the true value then the prior density.

Remark 3.8. In some references, e.g. [6, Theorem 3.1], a more general situation then in Remark 3.6 seems to be considered. Therein, the authors deal with the situation that there is some *fixed, true random variable* U_{true} with values in Q, such that the observations are samples of $V_{U_{true}}$. If one has a *prior* probability density π_0 on Q representing the information on/beliefs about U_{true} in advance of the observation(s) it is pointed out that for any observed datum v_{obs} of this kind one can use Bayes' Theorem of Inverse Problems as in Theorem 3.5 to get the posterior probability density for the prior density π_0, given the data v_{obs}.

Warning: The posteriori density one gets in this situation is the **same** as the posterior density one would get if one is considering Bayes' Theorem for the identification of a true value as in Remark 3.6. There are some situations, in which the computed posterior density can be a better approximation for U_{true} then the prior density, but contrary to the expectation, this does **not** hold typically. Instead, one can easily produce situations with some given and known U_{true} such that the posterior density is the **less accurate** approximation of U_{true}. especially if V_q is of the form described before Definition 3.2.

3.4 Adapting the identification problem to Bayes' Theorem

Adapting the situation considered in Section 3.2 to the framework of of Bayes' Theorem, we assume that there are independent random variables $\Gamma_{1,1}, \dots, \Gamma_{K_1,1}, \Gamma_{1,2}, \dots, \Gamma_{K_2,2}, \dots, \Gamma_{1,L}, \dots, \Gamma_{K_L,L}$ and samples $\gamma_{k,\ell}$ of $\Gamma_{k,\ell}$ such that (3.7) can be rewritten as

$$\Psi_{\mathcal{PI},c_{1,\ell},c_{2,\ell}}(v_{k,\ell}) + \gamma_{k,\ell} = \psi_{k,\ell}, \quad \forall\, k \in \{1, \dots, K_\ell\},\ \ell \in \{1, \dots, L\}. \tag{3.10}$$

In [7] it was assumed that $\Gamma_{2,1}, \dots, \Gamma_{K_1,1}, \Gamma_{2,2}, \dots, \Gamma_{K_2,2}, \dots, \Gamma_{2,L}, \dots, \Gamma_{K_L,L}$ have the distribution $N(0, \sigma^2)$ and that $\Gamma_{1,1}, \Gamma_{1,2}, \dots, \Gamma_{1,L}$ have the distribution $\mathcal{N}(0, (2\sigma)^2)$ for some given σ.

In view of the formulation of Bayes' Theorem as in [6, Theorem 3.1], see also Remark 3.8, it was believed that appropriate application of Bayes' Theorem should allow the determination of a posterior density such that $((c_{1,KDV,i}, c_{2,KDV,i}))_{i=1}^{58}$ as in Remark 3.1 could be considered as typical samples for a random variable with this density. An idea to achieve this aim was to subsequently apply Bayes theorem to (3.10) for the different values of $\ell \in \{1, 2, \dots, 58\}$, using the last computed posterior density as new prior density in each step.

But an inspection of this procedure yielded that the resulting density would represent the information that one would get for $c_{1,all}, c_{2,all} \in (0, \infty)$ such that (3.10) holds with $c_{1,\ell}$ replaced by $c_{1,all}$ and $c_{2,\ell}$

replaced by $c_{2,all}$ for all $\ell \in \{1,\dots,58\}$. Considering the likelihoods for $\sigma = 0.01$ and $\sigma = 0.02$, shown in [7, Fig 16, Fig 17], one observes that these functions are very small except for a quite small region, but the values for $((c_{1,KDV,i}, c_{2,KDV,i}))_{i=1}^{58}$ are distributed over a much larger region, see [7, Fig 14]. The pairs in the considered subset $((c_{1,KDV,i}, c_{2,KDVik}))_{i=30}^{55}$ of nice parameter pairs are also distributed over a much larger region, see [7, Fig 15].

Hence, with a normal choice for the priori density it will also hold that the posterior density is concentrated in a small region and a random variable with this density will not produce one of these sets of parameter values or a smaller one as typical samples.

4 Inverse and Forward UQ computations performed after completing [7]

4.1 Reformulation of problems to be considered for Bayes' Theorem, use of UQLab

In the following, Bayes' Theorem will be applied for appropriate parts of the Bayesian inverse problems (BIP) considered before and afterwards a convex combination of the resulting posterior densities will be determined.

To be able to deal with the posterior density and integrals involving this density, this density will be represented by samples resulting from dealing with BIPs using Markov-Chain-Monte-Carlo (MCMC)-computations. This has been done by applying *UQLab, the "The Framework for Uncertainty Quantification"*, see [13, 21] and `https://www.uqlab.com/`.

For subsets $\mathfrak{L}$ of $\{1,2,\dots,L\}$, it will be assumed that for all $\ell \in \mathfrak{L}$ it holds that the corresponding equations in (3.10) are evaluated with $c_{1,\ell}$ replaced by $c_{1,\mathfrak{L}}$ and $c_{2,\ell}$ replaced by $c_{2,\mathfrak{L}}$. Hence, we get

$$\Psi_{\mathcal{PI},c_{1,\mathfrak{L}},c_{2,\mathfrak{L}}}(v_{k,\ell}) + \gamma_{k,\ell} = \psi_{k,\ell}, \quad \forall\, k \in \{1,\dots,K_\ell\}, \ell \in \mathfrak{L}. \tag{4.1}$$

Moreover, we will assume that the independent random variables $\Gamma_{k,\ell}$ have the distribution $\mathcal{N}(0,\sigma_{\mathfrak{L}}^2)$ for all $k \in \{1,\dots,K_\ell\}$ and for all $\ell \in \mathfrak{L}$ for some appropriate $\sigma_{\mathfrak{L}} > 0$ that must be identified.

Hence, we consider $(\psi_{k,\ell})_{k=1,\dots,K_\ell,\,\ell\in\mathfrak{L}}$ as sample of $\left(\Psi_{\mathcal{PI},c_{1,\mathfrak{L}},c2,\mathfrak{L}}(v_{k,\ell}) + \Gamma_{k,\ell}\right)_{k=1,\dots,K_\ell,\,\ell\in\mathfrak{L}}$. Therefore, similar to [21, (1.17)], we get the likelihood

$$\begin{aligned} &L_{\mathfrak{L}}\left(\left(c_{1,\mathfrak{L}}, c_{2,\mathfrak{L}}, \sigma_{\mathfrak{L}}^2\right) \,\middle|\, (\psi_{k,\ell})_{k=1,\dots,K_\ell,\,\ell\in\mathfrak{L}}\right) \\ &= \prod_{\ell\in\mathfrak{L}} \prod_{k=1}^{K_\ell} \frac{1}{\sqrt{2\pi\sigma_{\mathfrak{L}}^2}} \exp\left(\frac{1}{2\sigma_{\mathfrak{L}}^2}\left(\psi_{k,\ell} - \Psi_{\mathcal{PI},c_{1,\mathfrak{L}},c_{2,\mathfrak{L}}}(v_{k,\ell})\right)^2\right). \end{aligned} \tag{4.2}$$

4.2 Approximation of length change and shift value

If one plans to use the results of inverse UQ to perform forward UQ and to reconstruct the measured length change, it is important to take into account the following considerations:

If one is considering a triple c_1, c_2, c_3 and would like to construct an approximation of the measured length change, it holds:

Variant 1 One could try to identify the initial internal state λ_0 describing the internal state of the specimen before the measurement started that corresponds to the 0-length change situation such that $\mathcal{G}_{c_1,c_2,c_3}[\lambda_0, I]$ with some shift should reproduce the measurements.

Variant 2 One could take advantage of the fact that in the situation considered in the measurements (also after the identification period is finished) it holds that there is a constant difference between $\mathcal{G}_{c_1,c_2,c_3}[\lambda_0, I]$ and $\mathcal{G}_{c_1,c_2,c_3}[0, I]$, with $\mathcal{G}_{c_1,c_2,c_3}[0, I]$ denoting the generalized Prandtl-Ishlinskiĭ-operator involving the Prandtl-Ishlinskiĭ-operator with trivial initial state as in Definition 2.4.b). Then, one just needs to determine some $shift$-value such that $\mathcal{G}_{c_1,c_2,c_3}[0, I] + shift$ is an approximation for the measured length change.

In the following, we will use Variant 2 and will determine the value for $shift$ by computing the output of the generalized Prandtl-Ishlinskiĭ-operator with trivial initial state at a time t being a minimum, i.e. $t \in \{t_1, t_3, \dots, t_{57}\}$ and compare the result with the measured length change L at this time.

Remark 4.1. If one is investigating the properties of the play-operator with trivial initial state with the modification that t_0 is the start of the considered time interval, see the discussions of reformulation of Sec. 2 in Sec. 3.2, it holds that

$$\mathcal{G}_{c_1,c_2,c_3}[0, I](t_0) = \mathcal{PI}_{\zeta_{c_1,c_2}}[0, \tanh(c_3 I)](t_0) = \Psi_{c_1,c_2}\left(\tanh(c_3 I(t_0)\right). \tag{4.3}$$

Moreover, following the discussion for the derivation of (3.6) for $i = 30$, we see that (2.6) is valid with $t_b = t_0$, $t = t_1$ and $u = \tanh(c_3 I)$. Using also (2.5) and simplifying the notations by using that the value of c_3 is fixed, we get

$$\mathcal{G}_{c_1,c_2,c_3}[0, I](t_1) = g_{c_1,c_2}(t_1), \text{ with} \tag{4.4}$$

$$g_{c_1,c_2}(t) := \Psi_{c_1,c_2}\big(\tanh(c_3 I(t_0))\big) - 2\Psi_{\mathcal{PI},c_{1,\mathfrak{L}},c_{2,\mathfrak{L}}}\left(\frac{1}{2}\left(\tanh\left(c_3 I(t)\right) - \tanh\left(c_3 I(t_0)\right)\right)\right), \quad \forall\, t \in [t_0, t_{59}]. \tag{4.5}$$

Taking advantage of the return-point memory of the generalized Prandtl-Ishlinskiĭ-operator and ignoring that there may be some differences since the values of the minima have some small variations, we get

$$\mathcal{G}_{c_1,c_2,c_3}[0, I](t_i) \approx g_{c_1,c_2}(t_i), \quad \forall\, i \in \{1, 3, 5, \dots, 57\}. \tag{4.6}$$

Now, considering the situation as in Sec. 4.1, for some subset $\mathfrak{L}$ of $\{1, \dots, L\}$, one equation or several equations involving $shift_{\mathfrak{L}}$ and one or several measurements of length changes needs/need to be formulated.

When doing forward UQ by considering samples representing the unknown parameters one also needs to somehow determine samples for $shift_{\mathfrak{L}}$.

Variant 1 If only one equation involving $shift_{\mathfrak{L}}$ is formulated, the following simple ansatz was used in previous computations: In the first step, one can perform inverse UQ using the likelihood formulated in Sec. 4.1 to generate a set of sample triple $\left(\left(c_{1,\mathfrak{L},n}, c_{2,\mathfrak{L},n}, \sigma^2_{\mathfrak{L},n}\right)\right)_{n=1}^N$ representing the joint posterior density for $c_{1,\mathfrak{L}}$, $c_{2,\mathfrak{L}}$, and $\sigma^2_{\mathfrak{L}}$. In the second step, one computes for each pair the corresponding sample value $shift_{\mathfrak{L},n}$ by inverting the equation discussed above. Afterwards, one could consider the samples quadruple $\left(\left(c_{1,\mathfrak{L},n}, c_{2,\mathfrak{L},n}, shift_{\mathfrak{L},n}, \sigma^2_{\mathfrak{L},n}\right)\right)_{n=1}^N$ as samples of some joint density representing $c_{1,\mathfrak{L}}$, $c_{2,\mathfrak{L}}$, $shift_{\mathfrak{L}}$, and $\sigma^2_{\mathfrak{L}}$.

Variant 2 The more complicated ansatz is to perform the inverse UQ already with $shift_{\mathfrak{L}}$ as a component and to use also the equation(s) for the shift value in the formulation of the Bayesian inverse problems (BIP). In the following, results for these kind of computations are presented.

To derive a BIP combining (4.1) with an equation for $shift_{\mathfrak{L}}$, we need to formulate one equation or several equations for this quantity such that the error can be estimated. Moreover, to implement this within the framework of UQLab, we need to formulate equations such that the error should be a sample of a random variable having the distribution $\mathcal{N}(0, \sigma_{\mathfrak{L}}^2)$.

To prepare this, we will consider the times for minima belonging to the data sets used to create $((v_{k,\ell}, \psi_{k,\ell}))_{k=1,\dots,K_\ell,\, \ell\in\mathfrak{L}}$. Hence, we consider

$$\mathfrak{L}^* := \left\{2i \,\middle|\, i \in \mathfrak{L},\, i \le 29\right\} \cup \left\{2(i-30)+1 \,\middle|\, i \in \mathfrak{L},\, i \ge 30\right\} \tag{4.7}$$

and assume now that

$$\eta^*_{k,j,\mathfrak{L}} := \mathcal{G}_{c_1,c_2,c_3}[0, I]\,(s_{k,j}) + shift_{\mathfrak{L}} - L\,(s_{k,j}) \tag{4.8}$$

for $k \in \{0, \dots, K_j^*\}$ and for $j \in \mathfrak{L}^*$ are samples for independent random variables all having the distribution $\mathcal{N}(0, \sigma^2_{\mathfrak{L},*})$ for some appropriate $\sigma_{\mathfrak{L},*} > 0$. (Here, we ignore that in view of (4.9) and other already requested independencies one may not be able to satisfy all the requested independencies.) Considering any $\ell \in \mathfrak{L}$ with $\ell < 29$ and any $k \in \{1, \dots, K_\ell\}$, we can recall (4.1), (3.4), and (2.6) to deduce that

$$\begin{aligned}
\gamma_{k,\ell} &= \frac{1}{2}\left(L(s_{k,2\ell}) - L(s_{0,2\ell})\right) - \Psi_{\mathcal{PI},c_{1,\mathfrak{L}},c_{2,\mathfrak{L}}}\left(\frac{1}{2}\left(\tanh\left(c_3 I(s_{k,2\ell})\right) - \tanh\left(c_3 I(s_{0,2\ell})\right)\right)\right) \\
&= \frac{1}{2}\left(L(s_{k,2\ell}) - \mathcal{G}_{c_{1,\mathfrak{L}},c_{2,\mathfrak{L}},c_3}[0, I]\,(s_{k,2\ell}) - shift_{\mathfrak{L}}\right) \\
&\quad - \frac{1}{2}\left(L(s_{0,2\ell}) - \mathcal{G}_{c_{1,\mathfrak{L}},c_{2,\mathfrak{L}},c_3}[0, I]\,(s_{0,2\ell}) - shift_{\mathfrak{L}}\right) \\
&= -\frac{1}{2}\eta^*_{k,2\ell,\mathfrak{L}} + \frac{1}{2}\eta^*_{0,2\ell,\mathfrak{L}}.
\end{aligned} \tag{4.9}$$

Recalling the assumption for $\eta^*_{i,2\ell,\mathfrak{L}}$ and Lemma 6.1, we deduce that the difference on the right-hand side is a sample of a random variable with distribution $N\left(0, \left(\frac{1}{\sqrt{2}}\sigma_{\mathfrak{L},*}\right)^2\right)$, and that this therefore also holds for $\gamma_{k,\ell}$.

Considering any $\ell \in \mathfrak{L}$ with $\ell > 29$ and any $k \in \{1, \dots, K_\ell\}$, we can recall (4.1), (3.5), and (2.6) to deduce with a similar computation that $\gamma_{k,\ell} = -\frac{1}{2}\eta^*_{0,2(\ell-30)+1,\mathfrak{L}} + \frac{1}{2}\eta^*_{k,2(\ell-30)+1,\mathfrak{L}}$. Recalling the assumption for $\eta^*_{i,2(\ell-30)+1,\mathfrak{L}}$ and Lemma 6.1, we deduce that this is a sample of a random variable with distribution $N\left(0, \left(\frac{1}{\sqrt{2}}\sigma_{\mathfrak{L},*}\right)^2\right)$.

Since it holds for all $\ell \in \mathfrak{L}$ and all $k \in \{1, \dots, K_\ell\}$, that $\gamma_{k,\ell}$ is by assumption a sample of a random variable with distribution $N\left(0, \sigma_{\mathfrak{L}}^2\right)$, but also a sample of a random variable with distribution $N\left(0, \left(\frac{1}{\sqrt{2}}\sigma_{\mathfrak{L},*}\right)^2\right)$, we deduce that

$$\frac{1}{\sqrt{2}}\sigma_{\mathfrak{L},*} = \sigma_{\mathfrak{L}}. \tag{4.10}$$

4.3 Bayesian inverse problem for data sets with increasing current

Considering the approximation for initial loading curves generated by following Remark 2.8 for the data sets with increasing current, as shown in Figure 6, we see that they all seem to approximate the same function on different intervals.

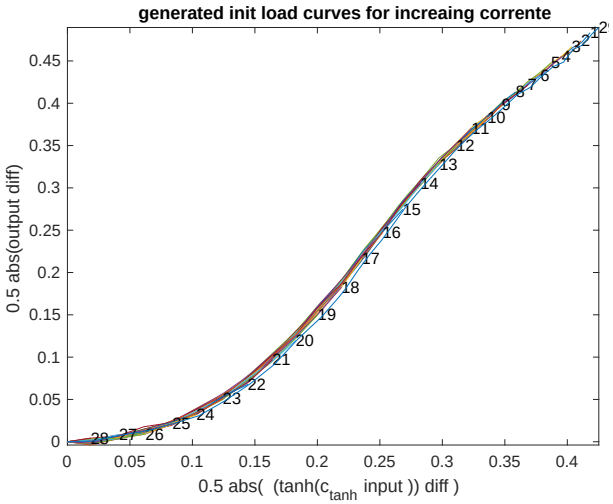

Figure 6: For the data sets involving increasing current, i.e. for every $i \in \{1, 2, \ldots, 29\}$, the approximation of an initial loading curve generated from the points $(v_{0,i}, \psi_{0,i}), (v_{1,i}, \psi_{1,i}), \ldots, (v_{K_i,i}, \psi_{K_i,i})$ following Remark 2.8 is shown.

To get samples representing the approximation of this function, a BIP for all data sets with increasing current is considered, i.e. we deal with $\mathfrak{L} = \{1, \ldots, 29\}$. Using (4.7), we see that $\mathfrak{L}^* = \{2, 4, \ldots, 58\}$.

Equation for $shift$:

In a situation without any noise or any model errors, one could compute the average over all values for $\mathcal{G}_{c_1,c_2,c_3}[0, I]$ evaluated in the 29 minima of the current at $t_1, t_3, \ldots, t_{57}$ and afterwards add $shift_{\{1,\ldots,29\}}$ to this average. The result should be equal to the average over all values for L evaluated in the 29 minima of the current.

In a situation with noise, one needs to consider the difference between these expressions and one has to check if it can considered as the sample of some random variable. Denoting the difference by $\delta_{\{1,\ldots,29\}}$, we get

$$\begin{aligned}\delta_{\{1,\ldots,29\}} &= \frac{1}{29}\sum_{i=1}^{29} \mathcal{G}_{c_1,c_2,c_3}[0, I]\,(t_{2i-1}) + shift_{\{1,\ldots,29\}} - \frac{1}{29}\sum_{i=1}^{29} L\,(t_{2i-1}) \\ &= \frac{1}{29}\sum_{i=1}^{29} \left(\mathcal{G}_{c_1,c_2,c_3}[0, I]\,(s_{1,2i}) + shift_{\{1,\ldots,29\}} - L\,(s_{1,2i})\right) = \sum_{i=1}^{29} \frac{1}{29}\eta^*_{1,2i,\{1,2,\ldots,29\}}.\end{aligned}$$

Recalling Lemma 6.1, the assumption on $\eta^*_{1,2i,\{1,2,\ldots,29\}}$, and (4.10), we see that the sum on the right-hand side is a sample for a random variable with distribution $\mathcal{N}\left(0, \sum_{i=1}^{29}\left(\frac{1}{29}\right)^2 \sigma^2_{\{1,2,\ldots,29\},*}\right) = \mathcal{N}\left(0, \frac{1}{29}\sigma^2_{\{1,2,\ldots,29\},*}\right) = \mathcal{N}\left(0, \frac{2}{29}\sigma^2_{\{1,2,\ldots,29\}}\right)$. In view of Lemma 6.1, we see that $\sqrt{\frac{29}{2}}\delta_{\{1,\ldots,29\}}$ would be a sample of a random variable with distribution $\mathcal{N}\left(0, \sigma^2_{\{1,2,\ldots,29\}}\right)$. Hence, using also (4.6),

we see that $\sqrt{\frac{29}{2}}\frac{1}{29}\sum_{i=1}^{29} L\left(t_{2i-1}\right)$ is a sample of a random variable with distribution $\mathcal{N}\left(\sqrt{\frac{29}{2}}\left(\frac{1}{29}\left(\sum_{i=1}^{29} g_{c_1,c_2}(t_{2i-1})\right) + shift_{\{1,\ldots,29\}}\right), \sigma^2_{\{1,2,\ldots,29\}}\right)$.

Attaching this random variable to $\left(\Psi_{\mathcal{PI},c_{1,\mathfrak{L}},c_{2,\mathfrak{L}}}\left(v_{k,\ell}\right) + \Gamma_{k,\ell}\right)_{k=1,\ldots,K_\ell,\,\ell=1,\ldots,29}$, ignoring in the following computations that the involved random variables are not independent, and considering (4.2) with $\mathfrak{L} = \{1, 2, \ldots, 29\}$, we get for the resulting likelihood

$$
\begin{aligned}
&L^{full}_{\{1,2,\ldots,29\}}\left(\left(c_{1,\{1,2,\ldots,29\}}, c_{2,\{1,2,\ldots,29\}}, shift_{\{1,2,\ldots,29\}}, \sigma^2_{\{1,2,\ldots,29\}}\right)\,\middle|\right.\\
&\qquad\left.\left(\left(\psi_{k,\ell}\right)_{k=1,\ldots,K_\ell,\,\ell=1,\ldots,29}, \sqrt{\frac{29}{2}}\frac{1}{29}\sum_{i=1}^{29} L\left(t_{2i-1}\right)\right)\right)\\
&= L_{\{1,2,\ldots,29\}}\left(\left(c_{1,\{1,2,\ldots,29\}}, c_{2,\{1,2,\ldots,29\}}, \sigma^2_{\{1,2,\ldots,29\}}\right)\,\middle|\,\left(\psi_{k,\ell}\right)_{k=1,\ldots,K_\ell,\,\ell=1,2,\ldots,29}\right)\\
&\quad\cdot L^*_{\{1,2,\ldots,29\}}\left(\left(c_{1,\{1,2,\ldots,29\}}, c_{2,\{1,2,\ldots,29\}}, shift_{\{1,2,\ldots,29\}}, \sigma^2_{\{1,2,\ldots,29\}}\right)\,\middle|\,\sqrt{\frac{29}{2}}\frac{1}{29}\sum_{i=1}^{29} L\left(t_{2i-1}\right)\right)
\end{aligned}
\tag{4.11}
$$

with

$$
\begin{aligned}
&L^*_{\{1,2,\ldots,29\}}\left(\left(c_{1,\{1,2,\ldots,29\}}, c_{2,\{1,2,\ldots,29\}}, shift_{\{1,2,\ldots,29\}}, \sigma^2_{\{1,2,\ldots,29\}}\right)\,\middle|\,\sqrt{\frac{29}{2}}\frac{1}{29}\sum_{i=1}^{29} L\left(t_{2i-1}\right)\right)\\
&= \frac{1}{\sqrt{2\pi\sigma^2_{\{1,2,\ldots,29\}}}}\\
&\quad\cdot\exp\left(\frac{1}{4\cdot 29\sigma^2_{\{1,2,\ldots,29\}}}\left(\sum_{i=1}^{29} L\left(t_{2i-1}\right) - \left(\sum_{i=1}^{29} g_{c_{1,\{1,2,\ldots,29\}},c_{2,,\{1,2,\ldots,29\}}}(t_{2i-1})\right) - 29shift_{\{1,2,\ldots,29\}}\right)^2\right).
\end{aligned}
\tag{4.12}
$$

Now, we use the product of appropriate uniform probability densities for $c_{1,\{1,2,\ldots,29\}}$, $c_{2,\{1,2,\ldots,29\}}$, $shift_{\{1,2,\ldots,29\}}$, and $\sigma^2_{\{1,2,\ldots,29\}}$ as prior density. Ignoring that the prior density should not involve any information derived by using the observations to be considered in Bayes' Theorem, the data pairs $\left(\left(c_{1,KDV,i}, c_{2,KDV,k}\right)\right)_{i=1}^{58}$ and the subset $\left(\left(c_{1,KDV,i}, c_{2,KDV,k}\right)\right)_{i=30}^{55}$ of nice data pairs computed in [7, Sec. 5] by using this observation, see Remark 3.1, have been used to define the prior. Moreover, the results of other inverse UQ computations for the considered observation have also been used.

1 The interval $[0, 100]$ used for $c_{1,\{1,2,\ldots,29\}}$ is chosen such that all values $\left(c_{1,KDV,i}\right)_{i=30}^{55}$ and almost all values $\left(c_{1,KDV,i}\right)_{i=31}^{58}$ are within this interval.

2 The interval $[0.00001, 4]$ used for $c_{2,\{1,2,\ldots,29\}}$ satisfies that most of the values $\left(c_{2,KDV,i}\right)_{i=30}^{55}$ and many of the values for $\left(c_{2,KDV,i}\right)_{i=1}^{58}$ are within this interval. The used upper bound 4 for $c_{2,\{1,2,\ldots,29\}}$ was derived by some heuristic considerations to ensure that there is still some

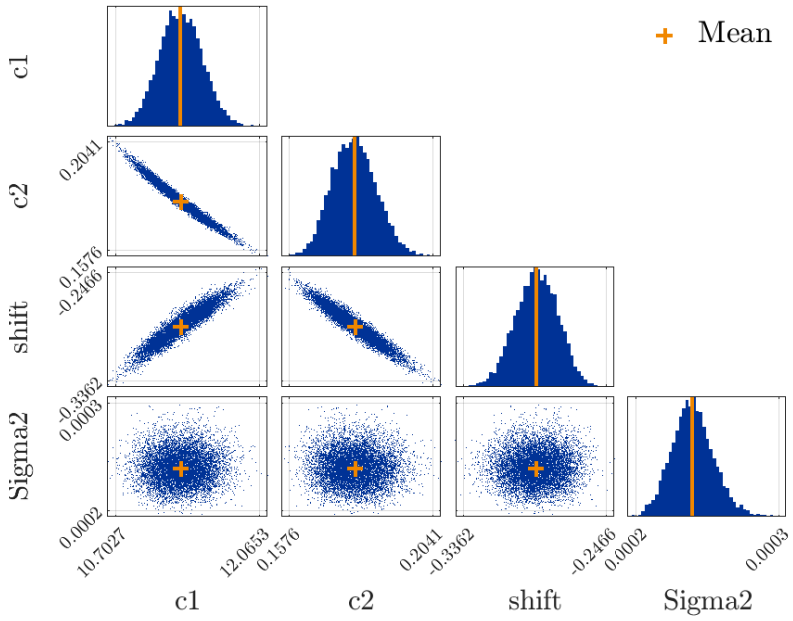

Figure 7: Scatter plot showing the samples $\left(c_{1,\{1,2,\ldots,29\},n},\ c_{2,\{1,2,\ldots,29\},n},\ shift_{\{1,2,\ldots,29\},n}\right)$ representing the posterior density following from dealing with all data sets for increasing current.

reasonable dependence of $L_{\{1,2,\ldots,29\}}\left((c_1, c_2, \sigma^2)\,\middle|\,(\psi_{k,\ell})_{k=1,2,\ldots,K_\ell,\,\ell=1,2,\ldots,29}\right)$ on c_2 on the complete interval.

3 Using data pairs for (c_1, c_2) derived by performing inverse UQ without the shift, and computing the $shift$ by inverting the considered equation, many samples for $shift$ had been computed. The interval $[-3, 3]$ is containing almost all of them.

4 In view of other results for dealing with the considered problem, using the interval $[0, 10^{-3}]$ to defined the prior density for $\sigma^2_{\{1,2,\ldots,29\}}$ seemed reasonable.

Following Remark 3.6, we are interested in the posterior density according to Bayes' Theorem of Inverse Problems as in Theo. 3.5.

To approximate the resulting posterior a set of samples is computed by using the *affine invariant ensemble algorithm*, see [21, Sec. 1.3.4], a special Markov-Chain-Monte-Carlo scheme, implemented in UQLab. An ensemble of 200 chains, denoted as *walker*, was considered, and 6000 iterations steps were performed. Afterwards, some walkers with improper evolutions were removed and the initial 90 % of the iterations steps in the remaining walkers were also removed. Hence, we got samples $\left(\left(c_{1,\{1,2,\ldots,29\},n},\ c_{2,\{1,2,\ldots,29\},n},\ shift_{\{1,2,\ldots,29\},n},\ \sigma^2_{\{1,2,\ldots,29\},n}\right)\right)_{n=1}^{115800}$.
These samples, i.e. a sufficient number of samples randomly selected from these samples are presented in the scatter plot in Fig. 7.

4.4 Result of forward UQ for data sets with increasing current

As pointed out in [21], the *posterior predictive density* can be computed by "averaging" the model output with additional noise over the posterior distribution. Thanks to (3.3) and Gauss summation, we

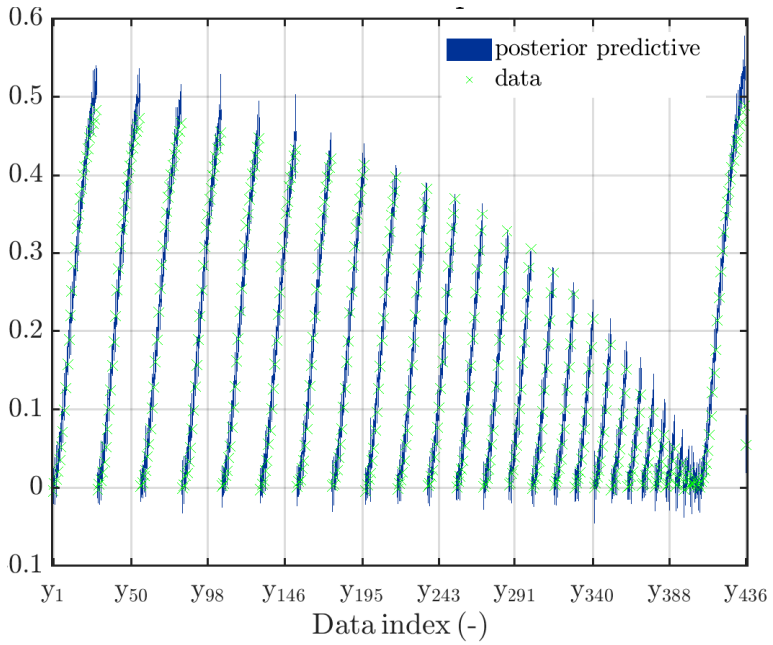

Figure 8: Violin plot of samples reflecting the posterior predictive density, derived by using some of the samples shown in Fig. 7 and marks for data points.

see that this is a density with $\sum_{\ell=1}^{29} K_\ell + 1 = \sum_{\ell=1}^{29} K_{2\ell}^* + 1 = \sum_{\ell=1}^{29} \ell + 1 = \frac{29*30}{2} + 1 = 436$ components.

Following [21, Sec. 1.2.6], one can generate samples for the posterior predictive density:

Starting with some sample $\left(c_{1,\{1,2,\ldots,29\},n},\, c_{2,\{1,2,\ldots,29\},n},\, shift_{\{1,2,\ldots,29\},n},\, \sigma^2_{\{1,2,\ldots,29\},n}\right)$ reflecting the posterior density, we get a sample $\xi_n \in \mathbb{R}^{436}$ reflecting the posterior predictive density by the following computation.

- Considering some index $k^* \in \{1,\ldots,435\}$, we define $\ell := \min\left\{\ell^* \in \{1,\ldots,29\} \middle| \sum_{i=1}^{\ell^*} K_i \geq k^*\right\}$ and afterwards define $k = k^*$ if $\ell = 1$, and $k = k^* - \sum_{i=1}^{\ell^*-1} K_i$ otherwise. Now, $\xi_n(k^*)$ will be the sum of $\Psi_{c_{1,\{1,\ldots,29\},n},c_{2,\{1,\ldots,29\}}}(v_{k,l})$ and a sample of a random variable with distribution $\mathcal{N}\left(0, \sigma^2_{\{1,\ldots,29\},n}\right)$.
- Moreover, $\xi_n(436)$ will be the sum of $\sqrt{\frac{29}{2}}\left(\frac{1}{29}\left(\sum_{i=1}^{29} g_{c_{1,\{1,\ldots,29\},n},c_{2,\{2,\ldots,29\},n}}(t_{2i-1})\right) + shift_{\{1,\ldots,29\}}\right)$ and a sample of a random variable with distribution $\mathcal{N}\left(0, \sigma^2_{\{1,\ldots,29\},n}\right)$.

The considered data vector is $\left(\psi_{1,1},\ldots,\psi_{K_1,1},\, \psi_{1,2},\ldots,\psi_{K_2,2},\, \ldots,\, \psi_{1,29},\ldots,\psi_{K_{29},29},\, \sqrt{\frac{29}{2}}\frac{1}{29}\sum_{i=1}^{29} L\left(t_{2i-1}\right)\right)$.

To somehow plot the posterior predictive density, one is randomly choosing 1000 samples $(\xi_{n_i})_{i=1}^{1000}$, and is showing a violin-plot for $(\xi_{n_i}(k))_{i=1}^{1000}$ for each $k \in \{1,\ldots,436\}$, see [15, Sec. uq_violinplot]. In the plot, marks for the value of the components of the data vector are also shown. In Figure 8 this

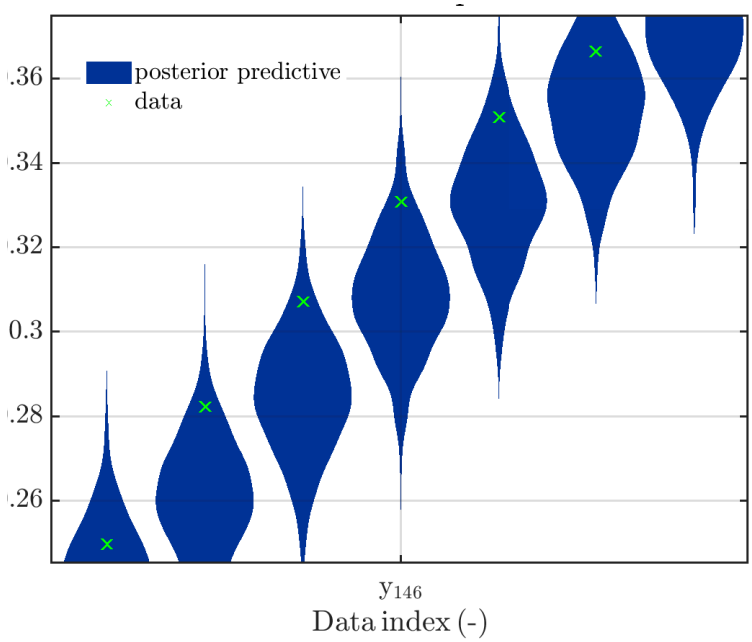

Figure 9: Blow-up of a part of Fig. 8

is shown for all 436 components, in the blow-up in Figure 9 one can see the result for the components $143, \ldots, 149$.

4.5 Bayesian inverse problem for data sets with decreasing current

Considering the approximation for initial loading curves generated for data sets with decreasing current, we see that the curves look different, see Fig. 10.

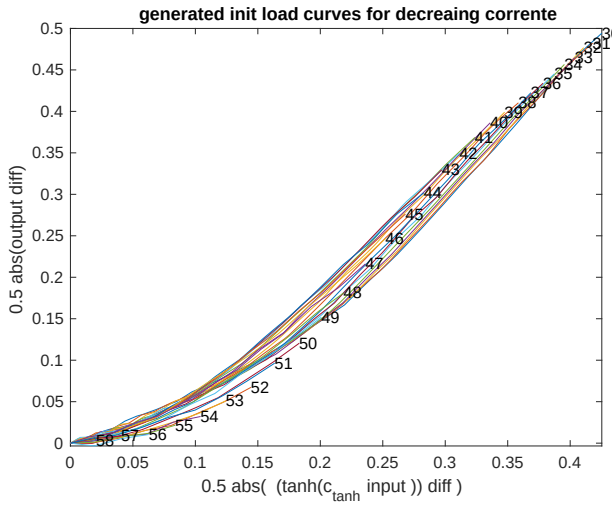

Figure 10: For the data sets involving decreasing current, i.e. for every $i \in \{30, 31, \ldots, 58\}$ the approximation of an initial loading curve generated from the points $(v_{0,i}, \psi_{0,i}), (v_{1,i}, \psi_{1,i}), \ldots, (v_{K_i,i}, \psi_{K_i,i})$ following Remark 2.8 is shown.

To get samples representing the approximation of these different functions, 29 Bayesian inverse problems are considered, one per data set with decreasing current.

Let any $i \in \{30, \dots, 58\}$ be given. Considering now $\mathfrak{L} = \{i\}$, we get from (4.7) that $\mathfrak{L}^* = \{2(i-30)+1\}$.

Equation for $shift_{\{i\}}$: The data set $((v_{k,i}, \psi_{k,i}))_{k=1}^{K}$ is derived from information on the current and the length change on the interval $[t_{2(i-30)}, t_{2(i-30)+1}]$. Since the current is decreasing on this interval, it is minimal at the end $t_{2(i-30)+1} = s_{K_i,2(i-30)+1}$ of the interval.

Since $\eta^*_{K_i,2(i-30)+1,\{i\}}$ is a sample of a random variable having the distribution $\mathcal{N}(0, \sigma^2_{\{i\},*})$, we deduce by recalling Lemma 6.1 and (4.10) that $\frac{1}{\sqrt{2}}\eta^*_{K_i,2(i-30)+1,\{i\}}$ is a sample of a random variable having the distribution $\mathcal{N}(0, \sigma^2_{\{i\}})$. Considering (4.8) for $k = K_i = K^*_{2(i-30)+1}$ and (4.6) we see that $\frac{1}{\sqrt{2}} L\left(t_{2(i-30)+1}\right)$ is a sample of a random variable with distribution $\mathcal{N}\left(\frac{1}{\sqrt{2}}\left(g_{c_{1,\{i\}},c_{2,\{i\}}}\left(t_{2(i-30)+1}\right) + shift_{\{i\}}\right), \sigma^2_{\{i\}}\right)$. Attaching this random variable to $\left(\Psi_{\mathcal{PI},c_{1,\{i\}},c_{2,\{i\}_2}}(v_{k,i}) + \Gamma_{k,i}\right)_{k=1}^{K_i}$, ignoring in the following computations that the involved random variables are not independent, and considering (4.2) with $\mathfrak{L} = \{i\}$, we get for the resulting likelihood

$$\begin{aligned} &L^{full}_{\{i\}}\left(\left(c_{1,\{i\}}, c_{2,\{i\}}, shift_{\{i\}}, \sigma^2_{\{i\}}\right) \,\middle|\, \left((\psi_{k,i})_{k=1}^{K_i}\,,\ \frac{1}{\sqrt{2}} L\left(t_{2(i-30)+1}\right)\right)\right) \\ &= L_{\{i\}}\left(\left(c_{1,\{i\}}, c_{2,\{i\}}, \sigma^2_{\{i\}}\right) \,\middle|\, (\psi_{k,i})_{k=1}^{K_i}\right) L^*_{\{i\}}\left(\left(c_{1,\{i\}}, c_{2,\{i\}}, shift_{\{i\}}, \sigma^2_{\{i\}}\right) \,\middle|\, \frac{1}{\sqrt{2}} L\left(t_{2(i-30)+1}\right)\right) \end{aligned} \tag{4.13}$$

with

$$\begin{aligned} &L^*_{\{i\}}\left(\left(c_{1,\{i\}}, c_{2,\{i\}}, shift_{\{i\}}, \sigma^2_{\{i\}}\right) \,\middle|\, \frac{1}{\sqrt{2}} L\left(t_{2(i-30)+1}\right)\right) \\ &= \frac{1}{\sqrt{2\pi\sigma^2_{\{i\}}}} \exp\left(\frac{1}{4\sigma^2_{\{i\}}}\left(L\left(t_{2(i-30)+1}\right) - g_{c_{1,\{i\}},c_{2,\{i\}}}\left(t_{2(i-30)+1}\right) - shift_{\{i\}}\right)^2\right). \end{aligned} \tag{4.14}$$

As in Sec. 4.3, we use the product of appropriate uniform probability densities for $c_{1,\{i\}}$, $c_{2,\{i\}}$, $shift_{\{i\}}$, and $\sigma^2_{\{i\}}$ as prior density. Moreover, similar to Sec. 4.3, the interval $[0, 100]$ is used for $c_{1,\{i\}}$, the interval $[-3, 3]$ is used for $shift_{\{i\}}$, and the interval $[0, 10^{-3}]$ is used for $\sigma^2_{\{i\}}$.

The interval $[0.00001, c_{2,up,\{i\}}]$ is used for $c_{2,\{i\}}$ with an upper bound $c_{2,up,\{i\}}$ derived by some heuristic considerations to ensure that there is still some reasonable dependence of $L_{\{i\}}\left((c_1, c_2, \sigma^2) \,\middle|\, (\psi_{k,\ell})_{k=1}^{K_i}\right)$ on c_2 on the complete interval. It holds that $c_{2,up,\{30\}} = 4$, $c_{2,up,\{40\}} = 3.29284$, $c_{2,up,\{50\}} = 1.76305,$, $c_{2,up,\{58\}} = 0.200779$.

As in Sec. 4.3, we follow Remark 3.6 and are interested in the posterior density according to Bayes' Theorem of Inverse Problems as in Theo. 3.5. Again, the affine invariant ensemble algorithm implemented in UQLab is applied.

In a first series of computations it turned out that for some values of i there are problems with the convergence of the algorithm; it seems that the scheme was not able to find the region wherein the corresponding likelihood is not very small since this region is much smaller then the overall considered domain.

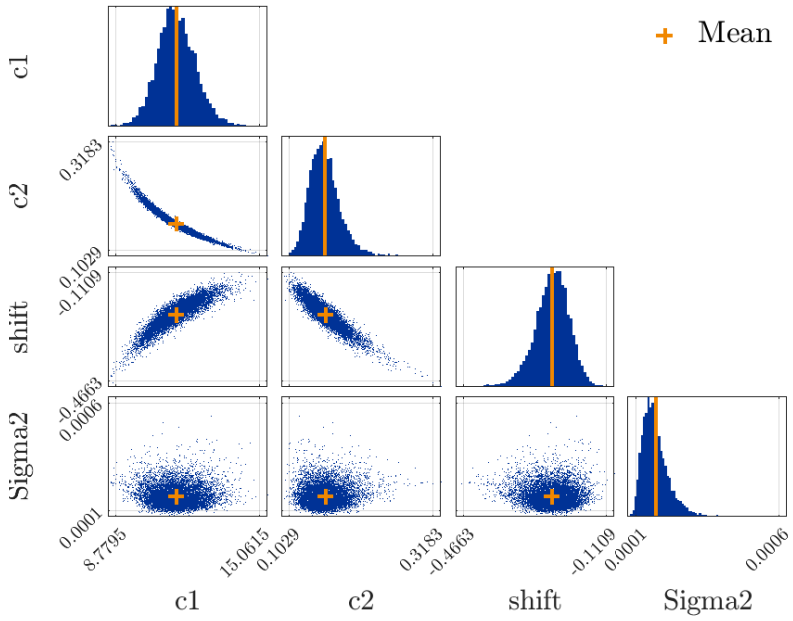

Figure 11: Resulting scatter plot of parameter samples $\left(c_{1,\{30\},n},\, c_{2,\{30\},n},\, shift_{\{30\},n},\, \sigma^2_{\{30\},n}\right)$ for the first data set with decreasing current, i.e. the data set No. 30.

Hence, to support the algorithm somehow, it was decided that the starting values for the walker should no longer be determined using samples of the random variable having the prior density and is therefore uniform on $[0, 100] \times [0.00001, c_{2,up,\{i\}}] \times [-3, 3] \times [0, 10^{-3}]$.

Instead, these initial values for the walkers were defined as the values of the walkers at the end of computations for some appropriate BIP performed as preparation. In this BIP it is requested that (4.1) is valid for $\mathfrak{L} = \{j\}$ for all $j \in \{30, \ldots, 59\}$, i.e. it is requested that (4.1) is valid for $\mathfrak{L} = \{30, \ldots, 59\}$. Moreover, is requested in this BIP that the result of an incorrect derivation of the equation for $shift$ in section 4.3 applies, wherein it is assumed incorrectly that $\delta_{\{1,\ldots,29\}}$ is a sample for a random variable with distribution $\mathcal{N}\left(0, \sigma^2_{\{1,2,\ldots,29\},*}\right)$. The resulting modification of the likelihood in (4.12) multiplied by $\prod_{\ell=30}^{58} L_{\{\ell\}}\left(\left(c_{1,\{30,\ldots,58\}}, c_{2,\{30,\ldots,58\}}, \sigma^2_{\{30,\ldots,58\}}\right) \middle| (\psi_{k,\ell})_{k=1}^{K_\ell}\right)$ results in the likelihood considered for dealing with this intermediate BIP. This BiP considered with the a priori density as for $i = 1$, being the same as the one considered in Section 4.3. This intermediate BIP is solved by applying the affine invariant ensemble algorithm with 200 walkers and 6000 iterations steps.

After removing 5 walkers with improper evolutions, the reaming 195 values were stored. These values were afterwards used as starting values for the 195 walkers used when the algorithm is applied to to deal with the BIP derived above for $\mathfrak{L} = \{i\}$.

4.6 Results of inverse and of forward UQ for first data set for decreasing current

Results of inverse UQ for the first data set with decreasing current, i.e. the data set No. 30, are samples $\left(c_{1,\{30\},n},\, c_{2,\{30\},n},\, shift_{\{30\},n},\, \sigma^2_{\{30\},n}\right)$ as shown in Fig. 11.

Figure 12: Violin plots for the first data set with decreasing current, i.e. for data set No. 30, showing the predictive description density for the predicted values of the initial loading curve (data index $1, \ldots, 29$) and for $\frac{1}{\sqrt{2}}$ of the predicted length change at t_1 (data index 30).

Similar to Sec. 4.4, we can generate samples for the posterior predictive density: Dealing with the first data set with decreasing current, i.e. with data set No. 30, it holds that the posterior predictive density has $K_{30} + 1 = 29 + 1 = 30$ components.

Starting from some sample $\left(c_{1,\{30\},n},\, c_{2,\{30\},n},\, shift_{\{30\},n},\, \sigma^2_{\{30\},n}\right)$ reflecting the posterior density, we get a sample $\xi_n \in \mathbb{R}^{30}$ reflecting the posterior predictive density by the following computation:

- For $k \in \{1, \ldots, 29\}$, $\xi_n(k)$ will be the sum of $\Psi_{c_{1,\{30\},n}, c_{2,\{30\},n}}\left(v_{k,30}\right)$ and a sample of a random variable with distribution $\mathcal{N}\left(0, \sigma^2_{\{30\},n}\right)$.
- Moreover, $\xi_n(30)$ will be the sum of $\frac{1}{\sqrt{2}}\left(g_{c_{1,\{30\},n}, c_{2,\{30\},n}}\left(t_1\right) + shift_{\{30\}}\right)$ and a sample of a random variable with distribution $\mathcal{N}\left(0, \sigma^2_{\{30\},n}\right)$.

The considered data vector is $\left(\psi_{1,30}, \ldots, \psi_{29,30},\ \frac{1}{\sqrt{2}} L\left(t_1\right)\right)$. In Fig. 12, the resulting violin plot and the data vector values are shown.

4.7 Further results of Bayesian inverse problem for data sets with decreasing current

It was observed that for the data sets $22, \ldots, 29$ with decreasing current, i.e. the data sets $51, \ldots, 58$ in the complete numbering, the MCMC-scheme has not reached convergence or may not reach convergence. Hence, only the data sets for the first 21 data sets with decreasing current will be considered, i.e. the data set $29, \ldots, 51$. A convex combination of the resulting posterior probability densities is approximated by randomly choosing some samples from each data set (number determined by some heuristic considerations involving the number of data points in the data sets), and afterwards merging all these samples to derive the *merged sample set for decreasing current*, see Fig. 13.

4.8 Merging sample sets for data sets with increasing current and decreasing current

A number of samples are randomly chosen from the sample set considered in the last section, and the same number of samples are randomly chosen from the sample set for increasing currents, see Fig. 7 and Fig. 15. Afterwards, both these sample sets are merged, see Fig. 14.

4.9 Result of forward UQ for merged data sets

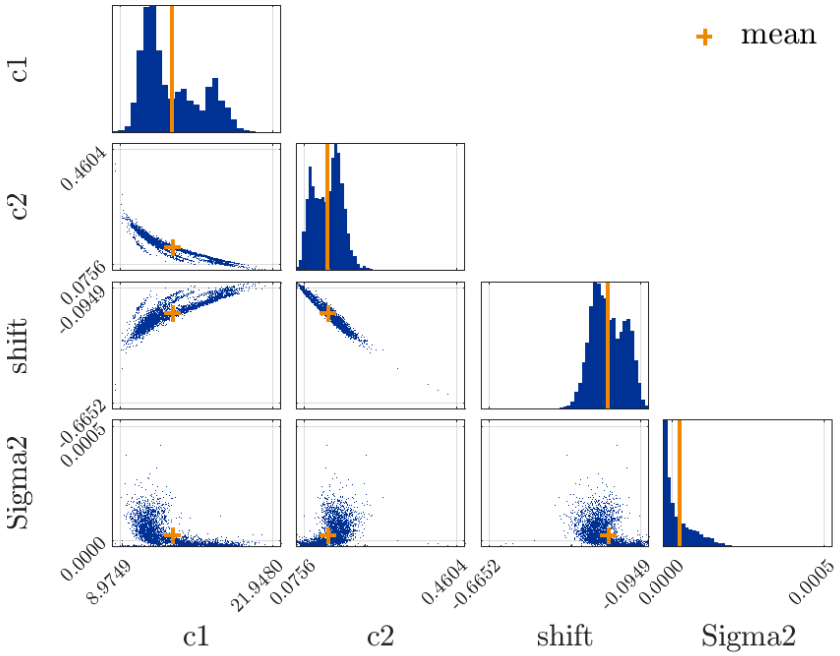

Figure 13: Scatter plot for merged sample set for decreasing current.

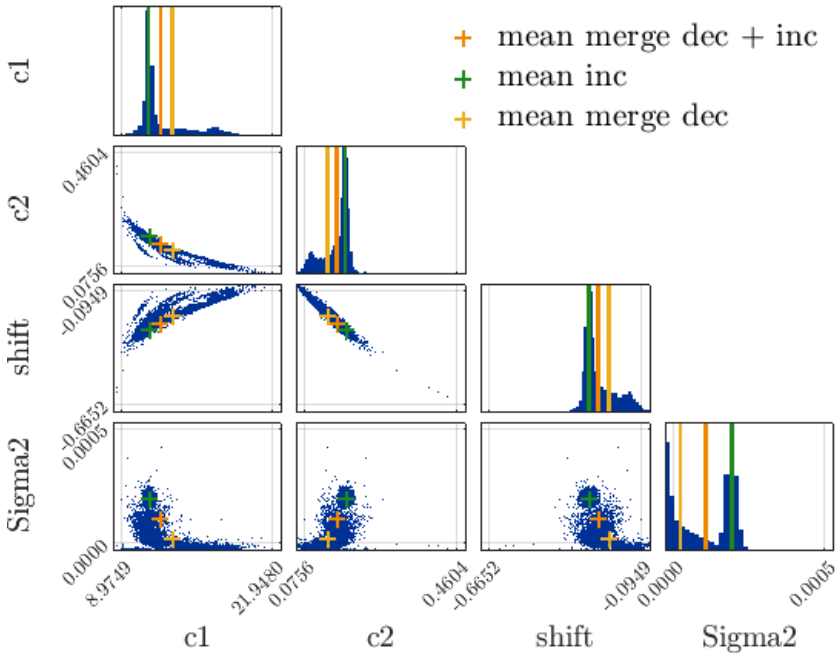

Figure 14: Samples derived by merging the samples for data sets with decreasing current, see Fig. 13, and those for data sets with increasing current, see Fig. 7 and also Fig. 15. The means of theses samples sets are also shown.

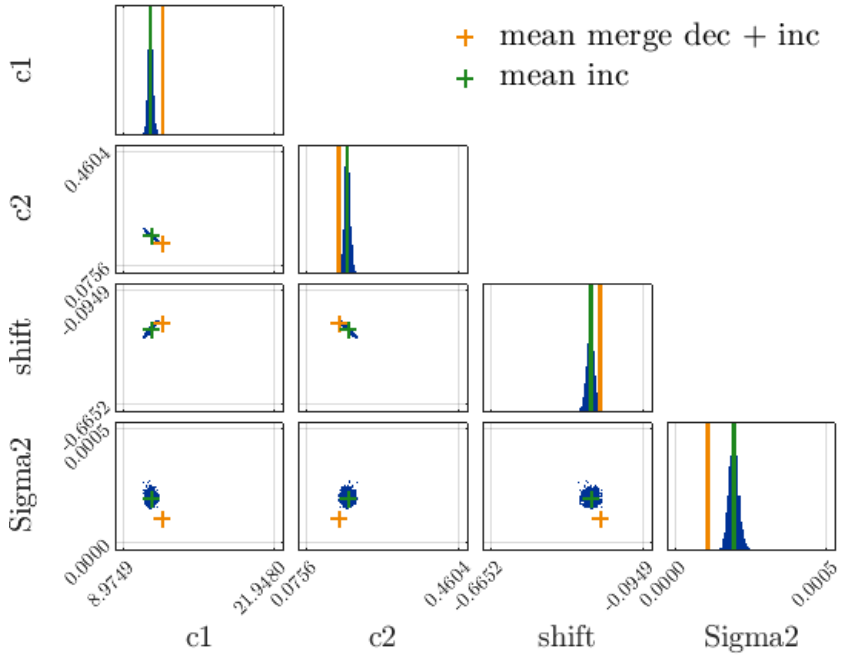

Figure 15: Scatter plot for the samples derived for 29 data sets with increasing currents is shown, and therein also the mean of these samples is also marked. These samples are also presented in Fig. 7. In the current figure the intervals for plotting c_1, c_2, $shift$ and σ^2 are the ones also used in Fig. 14. Moreover, the mean of the samples shown in Fig. 14, i.e. the merge of the samples for data sets with decreasing current and those for data sets with increasing current, is also marked.

In the following, we consider for every sample $(c_{1,n}, c_{2,n}, shift_n, \sigma_n^2)$ the function $[t_0, t_{58}] \ni t \mapsto \mathcal{G}_{c_{1,n},c_{2,n},c_3}[0, I](t) + shift_n$ for the given value for c_3 and the trivial initial state. This generates a set of sample functions.

Now, for each of the time steps t in the measurement, samples values are created by performing the following computation for all considered n: the sample function No. n is evaluated at t and $\sqrt{2}$ times a sample for a random variable with distribution $N(0, \sigma_n^2)$ is added.

Some quantiles values are computed from the resulting samples for posterior predictive density:

- the value of the 0.05–*quantiles at some time* t indicating that 5 % of all output samples values at time t are below this value and 95% are above this value,

- the value of the 0.95–*quantiles at some time* t indicating that 95 % of all output samples values at time t are below this value and 5% are above this value.

In Fig. 4, the measured data used for identification are shown. Now, the shown evolution of the measured length change in the identification period and the results of forward UQ can be compared, see Fig. 16.

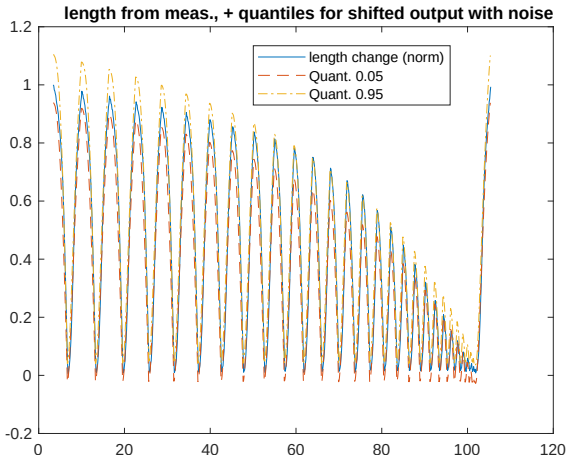

Figure 16: Result of forward UQ for merged data sets and measured length change during identification period.

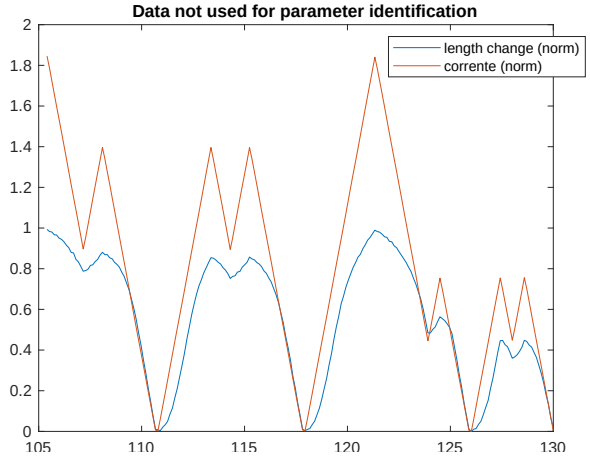

Figure 17: Evolution of current (input) and length change after identification period.

Now, the evolution of the measured length change after the identification period and the results of forward UQ are also compared, see Fig. 17.

- For the period not used for identification with 210 data points it holds that for 61 data points, i.e. for **29 %**, the measured value is not in the interval $[0.05$–quantile value, 0.95–quantile value$]$. The values for 27 points are smaller than the 5%–quantile value and the value for 34 are larger than the 95%–quantile value.

- For the period used for identification with 872 data points it holds that for 398 data points, i.e. for **46 %**, the measured value is not in the interval $[0.05$–quantile value, 0.95–quantile value$]$. The values for 182 points are smaller than the 5% quantile values and the values for 216 data points are larger than the 95% quantile values.

- Further investigations indicate that modeling using the generalized Prandtl-Ishlinskiĭ-operator produces a systematic error, somehow reflecting the systematic difference between the approximations for the initial loading curve for decreasing current and the corresponding approximations for increasing current.

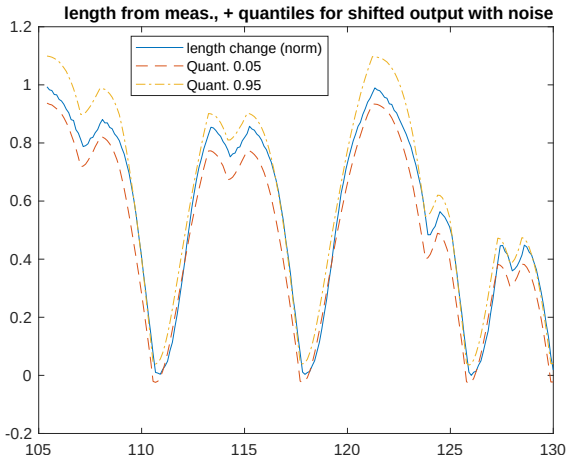

Figure 18: Result of forward UQ for merged data sets and measured length change, after identification period.

4.10 Consequences of the result of forward UQ

- The consideration in the subsection before indicate that one may have to replace the generalized Prandtl-Ishlinskiĭ-operator in the model by another one.
- FORC Diagrams are typically used to identify measures in so-called *Preisach-operators*, special kinds of hysteresis operators.
- In view of the model derivation in [3, Sec. 5], one should not use the generalized Prandtl-Ishlinskiĭ-operator to model the length change, but its *counterclockwise admissible potential* that is a Preisach-Operator. (Then it holds that the generalized Prandtl-Ishlinskiĭ-operator should be used to model the magnetization.) Some tests yield that using this operator generates a better approximation for the data generated for increasing current, but the approximation for the data generated for decreasing current time intervals gets worse. Since the data generated for decreasing current are the more relevant in this data set, it seems that one should consider some other operator instead.

5 Conclusion

Conclusion:
- Output of hysteresis operators depends on parameters, whose values may not be exactly known when modeling real world processes.
- Inverse UQ to identify these parameters and their uncertainty has been performed.
- Forward UQ has been performed with the sample derived from inverse UQ; the results have been compared to measurements.

6 Appendix

It holds, see e.g. [17, Theorm 4.21] or [5, Ex 4.9.3]:

Lemma 6.1. *Let $(\Omega, \mathfrak{F}, \mathbb{P})$ be a probability space. Let $X_1, \dots, X_n : \Omega \to \mathbb{R}$ be independent continuous random variables such that there is some $\sigma \in (0, \infty)$ with $X_i \sim \mathcal{N}(0, \sigma)$ for all $i \in \{1, \dots, n\}$. Let $a_1, \dots, a_n \in \mathbb{R} \setminus \{0\}$ be given. Then it holds that*

$$\sum_{i=1}^{n} a_i X_i \sim \mathcal{N}\left(0, \left(\left(\sqrt{\sum_{i=1}^{n} a_i^2}\right)\sigma\right)^2\right) = \mathcal{N}\left(0, \left(\sum_{i=1}^{n} a_i^2\right)\sigma^2\right). \tag{6.1}$$

References

[1] M. Al Janaideh, C. Visone, D. Davino, and P. Krejčí, *The generalized Prandtl-Ishlinskii model: relation with the Preisach nonlinearity and inverse compensation error*, 2014 American Control Conference (ACC) June 4-6, 2014. Portland, Oregon, USA, 2014.

[2] M. Brokate and J. Sprekels, *Hysteresis and phase transitions*, Springer, New York, 1996, Zbl 0951.74002, MR1411908.

[3] D. Davino, P. Krejčí, and C. Visone, *Fully coupled modeling of magneto-mechanical hysteresis through 'thermodynamic' compatibility*, Smart Mater. Struct. **22** (2013), no. 9.

[4] D. Davino and C. Visone, *Rate-independent memory in magneto-elastic materials*, Discrete and Continuous Dynamical Systems - Series S **8** (2015), no. 4, 649–691, Zbl 1302.93028, MR3356455.

[5] G. R. Grimmett and D.. Stirzaker, *Probability and random processes*, third ed., Oxford University Press, New York, 2001, MR2059709.

[6] J. Kaipio and E. Somersalo, *Statistical and computational inverse problems*, Applied Mathematical Sciences, vol. 160, Springer New York, NY, 2004, Zbl 1101.65008, MR2102218.

[7] O. Klein, D. Davino, and C. Visone, *On forward and inverse uncertainty quantification for models involving hysteresis operators*, Mathematical Modelling of Natural Phenomena **15** (2020), no. 53, 19, Zbl 07372583, MR4175380.

[8] O. Klein and P. Krejčí, *Outwards pointing hysteresis operators and asymptotic behaviour of evolution equations*, Nonlinear Anal. Real World Appl. **4** (2003), no. 5, 755–785, MR1978561.

[9] M. A. Krasnosel'skiĭ and A. V. Pokrovskii, *Systems with Hysteresis*, Springer-Verlag, Heidelberg, 1989, Zbl 0665.47038, MR0987431, Russian edition: Nauka, Moscow, 1983.

[10] P. Krejčí, *Hysteresis, convexity and dissipation in hyperbolic equations*, Gakuto Int. Series Math. Sci. & Appl., vol. 8, Gakkōtosho, Tokyo, 1996, Zbl 1187.35003, MR2466538.

[11] P. Krejčí, *Long-time behavior of solutions to hyperbolic equations with hysteresis*, Evolutionary equations. Vol. II, Handb. Differ. Equ., Elsevier/North-Holland, Amsterdam, 2005, pp. 303–370. Zbl 1098.35030, MR2182830.

[12] Peter M. Lee, *Bayesian statistics: An introduction*, fourth ed., John Wiley & Sons, Ltd., Chichester, 2012, Kindle Version.

[13] S. Marelli and B. Sudret, *UQLab: A framework for uncertainty quantification in matlab*, Vulnerability, Uncertainty, and Risk, American Society of Civil Engineers, jun 2014.

[14] I. D. Mayergoyz, *Mathematical models of hysteresis and their applications*, second edition ed., Elsevier, 2003.

[15] M. Moustapha, C. Lataniotis, P. Wiederkehr, , P.-R. Wagner, D. Wicaksono, S. Marelli, and B. Sudret, *UQLib user manual*, Tech. report, Chair of Risk, Safety and Uncertainty Quantification, ETH Zurich, Switzerland, 2022, Report UQLab-V2.0-201.

[16] Y. Pawitan, *In all likelihood: Statistical modelling and inference using likelihood*, Oxford science publications, OUP Oxford, 2001, Zbl 1013.62001.

[17] R. C. Smith, *Uncertainty quantification: theory, implementation, and applications*, Computational Science & Engineering, vol. 12, Society for Industrial and Applied Mathematics (SIAM), Philadelphia, PA, 2014, Zbl 1284.65019, MR3155184.

[18] T. J. Sullivan, *Introduction to uncertainty quantification*, Texts in Applied Mathematics, vol. 63, Springer, Cham, 2015, Zbl 1336.60002, MR3364576.

[19] A. Visintin, *Differential models of hysteresis*, Applied Mathematical Sciences, vol. 111, Springer, New York, 1994, Zbl 0820.35004, MR1329094.

[20] C. Visone and M. Sjöström, *Exact invertible hysteresis models based on play operators*, Physica B: Condensed Matter **343** (2004), no. 1, 148 – 152, Proceedings of the Fourth Intional Conference on Hysteresis and Micromagnetic Modeling.

[21] P.-R. Wagner, J. Nagel, S. Marelli, and B. Sudret, *UQLab user manual – Bayesian inversion for model calibration and validation*, Tech. report, Chair of Risk, Safety and Uncertainty Quantification, ETH Zurich, Switzerland, 2022, Report UQLab-V2.0-113.